NASA CR-1-34688

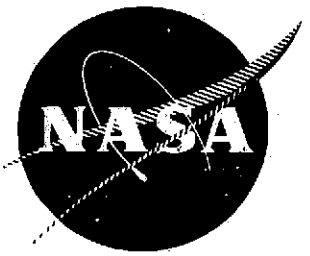

TOUGH CRYOGENIC ALLOYS FROM THE Fe-Mn AND Fe-Mn-Cr SYSTEMS

by

M. J. Schanfein, V. F. Zackay, and J. W. Morris, Jr.

prepared for

NATIONAL AERONAUTICS AND SPACE ADMINISTRATION

CONTRACT NGR 05-003-562

Department of Materials Science
and Engineering
University of California
Berkeley and Inorganic Materials Research Division
Lawrence Berkeley Laboratory
Berkeley, California 94720

Requests for copies of this report should be referred to

National Aeronautics and Space Administration
Office of Scientific and Technical Information
Attention: AFSS-A
Washington, D.C. 20546

NASA CR-1-34688

FINAL REPORT

TOUGH CRYOGENIC ALLOYS FROM THE Fe-Mn AND Fe-Mn-Cr SYSTEMS

by

M. J. Schanfein, V. F. Zackay, and J. W. Morris, Jr.

prepared for

NATIONAL AERONAUTICS AND SPACE ADMINISTRATION

September 18, 1974

CONTRACT NGR 05-003-562

Technical Management
NASA Lewis Research Center
Cleveland, Ohio
Materials Development Section
Joseph R. Stephens

Department of Materials Science
and Engineering
University of California
Berkeley and Inorganic Materials Research Division
Lawrence Berkeley Laboratory
Berkeley, California 94720

TOUGH CRYOGENIC ALLOYS FROM THE Fe-Mn AND Fe-Mn-Cr SYSTEMS

by

M. J. Schanfein, V. F. Zackay, and J. W. Morris, Jr.

ABSTRACT

By adjusting composition, metastable γ (austenite) and ε (hexagonal) martensite may be retained in Fe-Mn and Fe-Mn-Cr alloys and used to impact toughness through the TRIP mechanism. The resulting alloys have excellent toughness at cryogenic temperatures. The best alloys obtained to date are: Fe-20Mn, with σ_y = 79ksi and K_{IC} = 275 ksi$\sqrt{in}$ at 77°K, and Fc-16Mn-8Cr, with σ_y = 85ksi and K_{IC} = 72 ksi$\sqrt{in}$ at 77°K.

TOUGH CRYOGENIC ALLOYS FROM THE Fe-Mn AND Fe-Mn-Cr SYSTEMS

by M. J. Schanfein, V. F. Zackay, and J. W. Morris, Jr.

I. INTRODUCTION

Industrial demand for the storage and transportation of cryogenic liquids has brought about research effords to develope steels which exhibit both high strength and toughness at low temperatures. The bulk of this research has focused on steels of moderate nickel content. While excellent alloys have been obtained, the cost and potential scarcity of nickel creates a significant need for research toward cryogenic steels which are either low in nickel or nickel free. The present investigation was undertaken to assess the potential of Fe-Mn alloys for cryogenic use. These alloys are promising because of the possibility of retaining metastable phases in the microstructure (γ or ε-martensite) which transform on plastic strain, hence imparting toughness at cryogenic temperatures.

In the Fe-Mn system, a variety of substructural changes occur in the bcc lattice.[1] When the manganese content exceeds about 10%, austenitized and quenched alloys contain a hexagonal ε phase, and mixed $\alpha' + \varepsilon$ microstructures result.[2,3] When the manganese content is increased beyond 15% the face centered cubic γ phase is stabilized and resists transformation even when cooled to liquid nitrogen temperature; mixed $\alpha + \varepsilon + \gamma$ microstructures are obtained.

Recent studies in this laboratory and elsewhere[4-6] have shown that strain induced transformations can significantly raise the ductility and fracture toughness of alloys having metastable matrices. In the Fe-Mn system, the possible strain induced transformations are those of the hexagonal ε phase transforming during deformation to bcc α and of the retained austenite transforming to either ε or α, or both. Troiano and McGuire,[7] White and Honeycombe,[2] and more recently, Holden, et al.[3] found such phase transformations occurring during cold working of Fe-Mn alloys of intermediate manganese content. We sought to employ these transformations to impart good cryogenic toughness to nickel-free alloys.

II. EXPERIMENTAL PROCEDURES

A. Material Preparation

The alloys used for this investigation were prepared by induction melting high purity (99.9+) elemental starting materials in zirconium oxide crucibles first under a vacuum at 10^{-3} mm Hg and then under an argon atmosphere. From this melt three inch diameter ingots were cast in copper chill molds and cooled in an argon atmosphere. The ingots were homogenized for twenty-four hours at 1200°C in a vacuum and then furnace cooled. After being reheated to 1200°C they were upset forged to bars of dimensions 2-3/4 in. wide by 1-1/4 in. thick and air cooled. Material was cut from these bars to prepare one inch thick fracture toughness specimens. The remaining material was then rolled down to one half inch thickness at 1200°C and air cooled. Material was removed again for Charpy V-notch specimens and the remaining material was rolled down to one quarter inch thickness at 1200°C and air cooled. From this remaining material, flat tensile specimens were prepared.

The compositions and designations of the alloys are listed in Table I. All alloys (excepting the 16%Mn-0.05C alloy) contained 0.10% titanium and 0.05% aluminum, which were added to inactivate the dominant interstitials, carbon and nitrogen. The C + N content of the alloys was about 0.02%.

All of the material in rough cut test specimen dimensions was initially austenitized at 900°C for two hours in an air furnace (±5°C) and first ice brine quenched (10% salt solution) and then liquid nitrogen quenched. The sections were then machined into standard Charpy V-notch specimens, 0.15 in. thick flat tensile specimens, and 1 in. thick fracture toughness specimens (K_{IC}).

B. Mechanical Tests

The mechanical tests performed included hardness, tensile, Charpy impact, and fracture toughness tests. Hardness measurements were performed on Charpy V-notch specimens with a Wilson Rockwell Hardness tester. Charpy impact tests were carried out on a 225 ft-lb capacity impact testing machine as specified by ASTM procedure E-23-64. The tests were run at various testing temperatures with the use of liquid helium, nitrogen and isopentane, methyl alcohol and dry ice, and distilled water and ice.

Tensile properties were determined on an 11,000 lb. capacity Instrom Testing Machine at a crosshead speed of 0.1 cm/min. Tests were carried out at room temperature, -78°C (dry ice and methyl alcohol), and -196°C (liquid nitrogen).

Fracture toughness testing was performed following ASTM standard E399-72. The tests were carried out on a 300,000 lb. capacity MTS

machine using a 2-1/2 in. square, one inch thick crack-line loaded specimen. The specimens used were transverse sections cut from bars rolled to 1-1/4 in. thickness. The specimens were machined oversize, austenitized at 900°C for two hours, ice brine and liquid nitrogen quenched. They were then machined to final dimensions and fatigue pre-cracked. All specimens were pulled at -196°C (liquid nitrogen bath).

Of the compositions tested, only two met the plane strain fracture toughness criteria as specified by ASTM for the determination of K_{IC}. To analyze the other compositions, Witts Equivalent Energy approximation was used.[8] In this approximation, the lower bound fracture toughness is given by:

$$K_{IC} = \frac{P_Q\sqrt{A_1/A_2}\ f(a/w)}{B\sqrt{w}}$$

where P_Q is the load at any point on the curve in the linear portion and A_2 is the area under this part of the curve. A_1 is the area under the curve to maximum load and the quantities a, w, and B are respectively the crack length, the width, and the thickness of the specimen. The geometric shape factor f(a/w) is evaluated in the ASTM specifications.

C. Dilatometry

Dilatometry tests were performed to study the kinetics of the phase transformations during both heating and cooling. The specimens were one inch long by 1/4 inch in diameter with a 3/32 inch center hole to facilitate uniform heating. Dilatometric curves were determined at a heating and cooling rate of 630°C/hour in an air atmosphere tube furnace.

D. X-Ray Diffraction

Quantitative measurements of the amounts and types of phases present were conducted using a Picker X-ray diffractometer. The percentages of the phases present were estimated by comparing the integrated diffraction intensities of the (200) and (211) alpha peaks, (220) gamma peak, and (012) and (013) epsilon peaks from a copper K_α source with a LiF monochromator between the diffracted beam and detector. A check was made to determine if a high degree of preferred orientation existed in the X-ray specimens by taking Laue back reflection pictures using a Norelco vertical tube unit with a Mo source. The results were negative, but the specimens were run twice with the sample rotated 90° for the second run to minimize the effects of small amounts of preferred orientation. From the two runs, integrated intensities were averaged for every peak. Hot stage X-ray work was also performed using the Picker X-ray diffractometer to correlate the expansion during transformation, from the dilatometric graphs, to the epsilon to gamma

transformation. The surfaces of the X-ray specimens were carefully prepared following the same procedure ad that for the optical microscopic specimens up to but not including the etching.

E. Microscopy

Specimens used for optical metallographic observation were obtained from transverse sections of broken Charpy bars. These specimens were mounted in Koldmount, ground on Al_2O_3 emery paper to 000 grit, polished on a 6μ and then a 1μ diamond wheel and final polished using a 0.05μ Al_2O_3 solution in a syntron. Electropolishing was then performed on each specimen in a chromic acetic solution (400 ml acetic acid, 20 ml distilled water, 75 gm chromic trioxide) at 10°C until all surface scratches were removed. For those alloys without chromium a mixed acid reagent (20 ml HCl, 10 ml HNO_3, 10 ml H_2O_2, 20 ml glycerol) was applied for between 15 to 30 seconds. The electropolishing and application of mixed reagent were repeated several times to remove the deformed surface layer. Finally Klemm's reagent (100 ml cold saturated $Na_2S_2O_3$ (in H_2O) + 5 gm $K_2S_2O_5$) was applied for one minute. The chromium containing alloys presented a problem since this procedure did not reveal the microstructure. Instead, following the electropolish, ferric chloride (saturated solution of $FeCl_3$ in 20 ml HCl, 10 ml HNO_3, 20 ml glycerol) was applied for a maximum of 1 min. Repeated treatments were made using this new procedure to remove the deformed surface layer.

The fracture surfaces of broken Charpy specimens were examined with a Jeolco JSM-U3 scanning electron microscope (SEM) operated at 25 kV via secondary electron emission.

III. EXPERIMENTAL RESULTS AND DISCUSSION

A. Fe-Mn Alloys

The phase transformation temperatures of Fe-Mn alloys as determined by dilatometry are shown in Fig. 1, along with the results of previous investigators.[3,9] When these alloys were cooled from the austenite phase a variety of complex microstructures resulted. The as-quenched structure of low manganese alloys cooled to LN (-196°C) was entirely bcc. As has been reported,[1] the substructure morphology changes from equiaxed ferrite (α) to lath and plate martensites (α') as the manganese content is increased to about 12%. In Figs. 2 and 3 are shown micrographs illustrating the structure of the Fe-Mn alloys of the present study. An example of the typical "massive" lath martensite microstructure of the 4, 8, and 12% Mn alloys are shown in Figs. 2(a), (b), and 3(a). In alloys with manganese contents greater than 12%, increasing amounts of the hexagonal ε phase formed. Within the 12%-20% Mn composition range, various complex microstructures, consisting of mixtures of the α', ε and γ phases, were obtained. Examples of these mixed microstructures

are shown in Figs. 3(c,e). The microstructure of the 16% Mn alloy (Fig. 3(c)) was predominantly $\alpha' + \varepsilon$ while that of the 20% Mn alloy was entirely $\varepsilon + \gamma$ (Fig. 3(e)).

The sequence of structural changes in Fe-Mn alloys was similar to that in the more familiar Fe-Ni system, except for the occurrence, in Fe-Mn alloys, of the hexagonal ε phase. This phase has been found only in those alloy systems where solute additions decrease the stacking fault energy of the austenite to low values. At low stacking fault energies the driving force necessary for the $\gamma \rightarrow \varepsilon$ transformation is reduced below that of the $\gamma \rightarrow \alpha'$ transformation and a metastable ε phase forms.[10]

The Charpy impact toughness is plotted as a function of temperature in Fig. 4 for the various Fe-Mn alloys (as austenitized). The fracture surfaces of the Charpy bars broken at both room (22°C) and LN(-196°C) temperatures are shown in Figs. 5 and 6, and correspond to the microstructures illustrated in Figs. 2 and 3. The room temperature Charpy fractures of the 4%Mn, 8%Mn, 12%Mn, 16%Mn, and 20%Mn alloys revealed the dimpled rupture characteristic of ductile behavior. In the liquid nitrogen (-196°C) tests the 4%Mn and 8%Mn alloys exhibited features of cleavage failure whereas the 12%Mn alloy showed intergranular failure with dispersed areas of dimple rupture. These areas may correspond to the small amounts of epsilon and gamma as revealed by X-ray analysis. Since they would preferentially appear at grain boundaries and are substantially weaker than the alpha phase, it is plausible that these areas are responsible for the intergranular failure. The 16%Mn and 20%Mn alloys showed predominantly dimpled rupture with some quasicleavage.

In Fig. 7 is shown a plot relating the DBTT to manganese content. The DBTT was measured as the temperature at which the Charpy impact energy had fallen to one-half its shelf value. It is evident from Fig. 7 that as the manganese content increased the DBTT first increased (up to approximately 8%Mn) and then decreased rapidly (at a rate of $\sim$ 21°C/at.%Mn).

The results of cryogenic fracture toughness tests on these Fe-Mn alloys are shown in Table V. The 4%Mn and 12%Mn alloys were relatively brittle in these tests, and plane strain conditions were easily obtained. The 16%Mn and 20%Mn alloys were not in plane strain conditions. The K_{IC} values shown in the table were computed using the equivalent energy approximation (equation (1)). Both the 16%Mn and 20%Mn alloys exhibited outstanding toughness at liquid nitrogen temperatures. The fracture surfaces are shown in Figs. 11(a,b) and 12(a,b). The fracture surfaces are flat and rather brittle in appearance, despite the high toughness of the samples pictures in Figs. 12(a,b). These results are typical of alloys toughened by incorporating phases which transform during deformation (the TRIP mechanism).

X-ray analysis was performed to determine the quantities of the phases present. The results of this X-ray phase analysis, Table III, indicated that the 4%Mn and 8%Mn alloys were completely bcc while the 12%Mn, 16%Mn, and 20%Mn alloys contained increasing amounts of the ε and

γ phases. The 16%Mn alloy had an $\alpha + \varepsilon + \alpha$ mixed microstructure while the 20%Mn alloy had an $\varepsilon + \gamma$ mixed microstructure. Combining the results of the X-ray analysis and DBTT determinations leads to the conclusion that the ε or γ or both phases are responsible for the improved low temperature toughness of the higher manganese alloys (12 to 20%Mn). In terms of the $(\varepsilon + \gamma)$ phases present, the DBTT decreased at a rate of 1/3°C/vol% $(\varepsilon + \gamma)$.

Besides the low DBTT, an adequate yield strength must also be developed in an alloy which is to be considered for cryogenic applications. The yield and tensile strengths, elongation, and reduction in area both at room, dry ice, and liquid nitrogen temperatures are listed in Table IV. In addition, plots of these properties as a function of manganese content are shown in Figs. 8 and 9. From these figures, it can be seen that the 4%Mn, 8%Mn, and 12%Mn alloys with bcc matrices exhibited fairly high yield strength but rather poor elongation. As the manganese content of the alloys was increased, the amount of the hexagonal ε phase also increased. This in turn was associated with a considerable decrease in yield strength. The room temperature yield strength of the 16%Mn alloy, which had almost 40% ε, was only 30 ksi. Increase in the manganese content to 20% resulted in stabilization of the γ phase, and no α phase was present in the as-quenched alloy. The alloy contained 66% ε and 34% γ. At room and LN temperatures, yield strengths of the 20%Mn alloy were 60 and 78 ksi respectively, and elongations were 43% and 62% respectively. Thus it appeared that with increasing amounts of ε in a primarily α microstructure the yield strength decreased; however, when the microstructure was predominantly ε, and γ replaced α, the yield strength decreased; however, when the microstructure was predominantly ε, and γ replaced α, the yield strength increased.

The results of X-ray analysis (Table III) clearly indicated that during tensile testing the ε phase in the 16%Mn alloy transformed to α. It was probable that a stress induced martensitic transformation of ε to α contributed to the low yield strength of the 16%Mn alloy. Stress induced transformations have been reported in several metastable austenitic steels of low austenite stability.[6,11] The increase in manganese content to 20% apparently resulted in two changes. First, it led to the elimination of the α phase transformation and the retention of the γ phase. As a result, the alloy consisted of a mixture of ε and γ phases of apparently comparable strengths, thus preventing localized flow in either phase. Second, the ε phase in the 20%Mn alloy was more stable than that in the 16%Mn alloy, thus minimizing the possible occurrence of a stress induced transformation. The higher stability of the 20%Mn alloy compared to that of the 16%Mn alloy was evident from the observation that during tensile testing a greater volume fraction of ε transformed to α in the latter alloy (see Table III).

It follows from the above data that Fe-Mn alloys may be made tough at cryogenic temperatures by incorporating metastable γ or ε-martensite in the microstructure. The drawback in this approach is the appreciable

drop in alloy tensile strength. This problem may be partially overcome through the addition of chromium, as shown in the following section.

B. Fe-Mn-Cr Alloys

The relationship between microstructure, strength and toughness was also examined in several Fe-Mn alloys containing 8%Cr. The relative proportions of the α, ε and γ phases in the chromium-containing alloys before and after tensile testing are indicated in Table III. Figure 9 shows the Charpy impact toughness as a function of temperature for the various as austenitized Fe-Mn alloys with and without chromium.

The fracture surfaces of the Charpy bars broken at both room (22°C) and liquid nitrogen (-196°C) temperatures are shown in Fig. 10 and correspond to the microstructures illustrated in Figs. 3(b,d,f). These fracture surfaces exhibited the same behavior at both room and liquid nitrogen temperatures as the corresponding alloys without chromium.

Figures 11 and 12 show the fracture surfaces of the fracture toughness (K_{IC}) specimens tested at liquid nitrogen temperature. It is interesting to note that no large shear lips were present on any of the specimens and they were in fact very difficult to observe even in the 20%Mn and 20%Mn-8%Cr alloys.

The results suggested that chromium additions to Fe-Mn alloys favored the transformation of ε and γ to the α phase during deformation.

In the as-quenched condition, the volume fraction of the α phase in the 12%Mn-8%Cr alloy was reduced by approximately 7% from the 12%Mn alloy. This is reflected in the slightly lower yield strength, shift of DBTT to a lower temperature (see Fig. 9) and increase in fracture toughness (K_{IC}) (see Table V). For the 16%Mn-8%Cr alloy the volume fraction of the α phase was almost twice that in the 16%Mn alloy. The yield strength of the chromium-containing alloy was correspondingly higher. In spite of the greater volume fraction of α (and the smaller volume fraction of ε) and the higher yield strength, the chromium containing alloy had approximately the same DBTT as the alloy without chromium (see Fig. 9). However, the CVN shelf energy was lower and the fracture toughness (see Table V) was reduced to slightly less than half.

In the 20%Mn-8%Cr alloy, there was a slight increase in gamma over the 20%Mn alloy. An additional decrease in the DBTT was observed (see Fig. 9) with little loss in strength and the fracture toughness remained unchanged (see Table V).

From these three alloys with 8%Cr added, the chromium appears to favor the gamma phase in the 12 and 20%Mn alloys. In the 16%Mn-8%Cr alloy, even though the alpha was preferentially favored (which agrees with the previous dilatometry data for cooling) over either epsilon or gamma, the gamma was still favored over epsilon since the former was

only reduced by 24% as opposed to 41% for the latter. The reasons for this behavior are not well understood. Nevertheless, it was evident that the 8% chromium addition to the 16%Mn alloy was beneficial for attaining a superior combination of strength and toughness. These properties coupled with the possible enhanced corrosion resistance of the 16%Mn-8%Cr alloys may be desirable in cryogenic applications.

CVN specimens of the 20%Mn alloys with and without chromium were also broken in liquid helium, using a technique developed by S. Jin.[12] Both alloys absorbed approximately 74 ft-lbs, indicating that significant toughness is retained to near liquid helium temperature (5-6°K).

C. Preliminary Results of the Effects of Carbon on a Mixed Structure

In addition to the above alloys, one alloy of 16%Mn-0.05%C was prepared and tensile (Table IV) and CVN energy (Fig. 13) tests were performed. The main reason for the addition of carbon was to evaluate its effect on the amounts of the phases present, on the strength, and on the toughness. From the X-ray data in Table III it can be seen that the carbon favored the formation of the epsilon and gamma phases. The gamma phase was increased by 49% and the epsilon by 26% over that in the 16%Mn alloy. The yield strength at room temperature was increased by 75% while at L.N. temperature, the yield strength was increased by 36% (Table IV) and the CVN energy was relatively unchanged except at LN temperatures where the 16%Mn alloy absorbed only 25 ft/lbs, compared with 42 ft/lbs for the 16%Mn-0.05%C alloy. The scanning electron micrographs of the CVN fracture surfaces show dimpled rupture at room temperature (22°C) and dimpled rupture and quasicleavage at LN (-196°C) temperature (Fig. 14).

From the above results it can be seen that carbon had the beneficial effects of raising the yield strength while leaving the CVN energy relatively unchanged.

IV. CONCLUSIONS

1. Fe-Mn alloys can be made to show excellent toughness at cryogenic temperatures. The toughening mechanism is a TRIP mechanism based on the retention of metastable γ and ε-martensite in the microstructure of alloys containing $\sim$16-$\sim$20%Mn. An Fe-20%Mn alloy exhibited a fracture toughness, K_{IC} (equivalent energy approximation), of 275 ksi$\sqrt{in}$ at a yield strength, σ_y, of 78 ksi at 77°K. The ductile-brittle transition temperature of this alloy in Charpy impact tests was below 6°K.

2. An 8%Cr addition strengthens the alloy without catastrophic loss in toughness. An Fe-16%Mn-8%Cr alloy showed a K_{IC} (equivalent energy approximation) of 72 ksi$\sqrt{in}$ at yield strength 85 ksi at 77°K. The chromium addition favored the transformation of ε and γ to the α phase during deformation.

REFERENCES

(1) Roberts, M. J., Metallurgical Transactions, Amer. Soc. for Metals, Vol. 1, 1970, pp. 3287-3294.

(2) White, C. H. and Honeycombe, R. W. R., J. Iron and Steel Inst., Vol. 200, June 1962, pp. 457-466.

(3) Holden, A., Bolton, J. D. and Petty, E. R., J. Iron and Steel Inst., Vol. 209, Sept. 1971, pp. 721-728.

(4) Gerberich, W. W., Hemmings, P. L. and Zackay, V. F., Metallurgical Transactions, Amer. Soc. for Metals, Vol. 2, 1971, pp. 2243-2253.

(5) Antolovich, S. D. and Singh, B., Metallurgical Transactions, American Society for Metals, Vol. 2, 1971, pp. 2135-2141.

(6) Bhandarkar, D., Zackay, V. F. and Parker, E. R., Metallurgical Transactions, American Society for Metals, Vol. 3, 1972, pp. 2619-2631.

(7) Troiano, A. R. and McGuire, F. T., Transactions of the A.S.M., Amer. Soc. for Metals, Vol. 31, 1947, p. 355.

(8) Riccardella, P. D. and Swedlow, Heavy Steel Technology Program Technical Report No. 33, WCAP 8224, October 1973, Section 2, p. 5.

(9) Hansen, M., Constitution of Binary Alloys, McGraw-Hill, New York, 1958, pp. 664-668.

(10) Breedis, J. F. and Kaufman, L., Metallurgical Transactions, American Society for Metals, Vol. 2, 1971, pp. 2359-2371.

(11) Reed, R. P. and Guntner, C. J., Transactions of the Metallurgical Society of the American Institute of Mining and Metallurgical Engineers, Vol. 230, 1964, pp. 1713-1720.

(12) Jin, S., Horwood, W. A., Morris, Jr., J. W. and Zackay, V. F., Advances in Cryogenic Engineering, Vol. 19, 1974, p. 373.

Table I. Chemical Compositions of Alloys.

Designation	Composition, wt%			
	Mn	Cr	C	Fe
4% Mn	4.1	--	--	Bal.
8% Mn	8.1	--	--	Bal.
12% Mn	12.1	--	--	Bal.
16% Mn	16.0	--	--	Bal.
20% Mn	19.5	--	--	Bal.
12% Mn 8% Cr	12.2	7.7	--	Bal.
16% Mn 8% Cr	15.8	7.9	--	Bal.
20% Mn 8% Cr	20.2	7.9	--	Bal.
16% Mn	16.3	--	0.05	Bal.

Table II. Hardness (Rockwell C Scale).

Designation	Without Chromium	With Chromium	With Carbon
4% Mn	10.1	----	----
8% Mn	17.8	----	----
12% Mn	24.7	26.7	----
16% Mn	10.9	18.8	19.0
20% Mn	15.4	14.6	----

Table III. Determination of Volume Percent of Phase Present by X-ray Analysis.

Designation	Prior to Tensile Tests			After Tensile Testing at 25°C			After Tensile Testing at -196°C		
	α	ε	γ	α	ε	γ	α	ε	γ
4% Mn	100	--	--	100	---	---	100	--	--
8% Mn	100	--	--	100	---	---	100	--	--
12% Mn	94	6	--	100	---	---	100	--	--
16% Mn	30	45	25	92	---	8	95	--	5
20% Mn	---	66	34	18	51	31	39	29	32
12% Mn-8% Cr	88	8	4	100	---	---	100	--	--
16% Mn-8% Cr	54	27	19	100	---	---	100	--	--
20% Mn-8% Cr	---	61	39	27	42	31	62	21	17
16% Mn-0.05 C	8	54	38	77	13	10	39	--	7

Table IV. Tensile data.

Designation	Temp. (°C)	Yield (ksi)	Ultimate (ksi)	% Elong.	Percent Reduction in Area
4% Mn	22	82.1	87.2	11	73
	-78	89.8	98.0	14	73
	-196	130.7	139.4	15	33
8% Mn	22	92.1	96.5	10	68
	-78	104.2	110.5	10	63
	-196	139.6	145.4	1	1
12% Mn	22	88.2	127.2	17	63
	-78	107.0	147.8	18	64
	-196	155.5	197.3	19	45
16% Mn	22	29.4	101.2	40	71
	-78	34.4	125.0	40	71
	-196	48.0	170.5	45	60
20% Mn	22	60.9	101.4	43	70
	-78	68.8	119.2	45	71
	-196	78.2	152.7	62	67
12% Mn-8% Cr	22	85.7	131.1	17	66
	-78	101.9	152.0	18	64
	-196	142.9	205.0	11	8
16% Mn-8% Cr	22	44.7	109.1	20	68
	-78	73.8	134.2	31	67
	-196	84.9	185.8	34	56
20% Mn-8% C	22	57.5	95.0	52	75
	-78	66.5	114.3	51	72
	-196	73.7	153.4	60	63
16% Mn-0.05 C	22	51.2	124.6	40	67
	-78	60.1	139.9	44	70
	-196	65.4	178.9	49	60

Table V. Fracture Toughness (K_{IC}) at 77°K.

Designation	Without Chromium	With Chromium
4% Mn	5.0	--
12% Mn	29.8	34.0*
16% Mn	157.4*	72.0*
20% Mn	275.3*	274.9*

*Calculated using Witt's equivalent energy theory (Equation (1)).

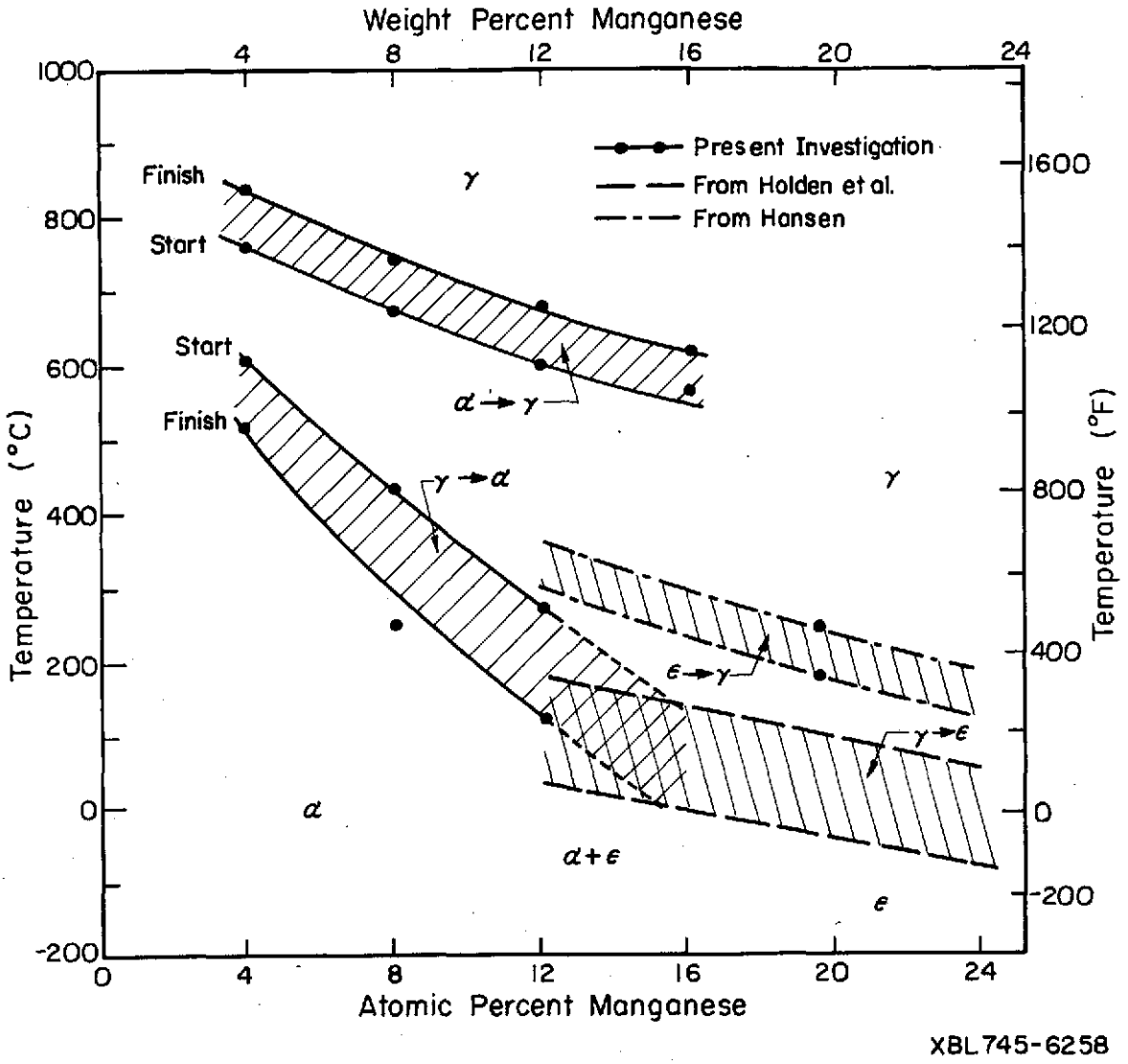

Fig. 1. Phase transformation temperatures for Fe-Mn alloys of the present investigation. Also shown are some results of other investigations.[12,18]

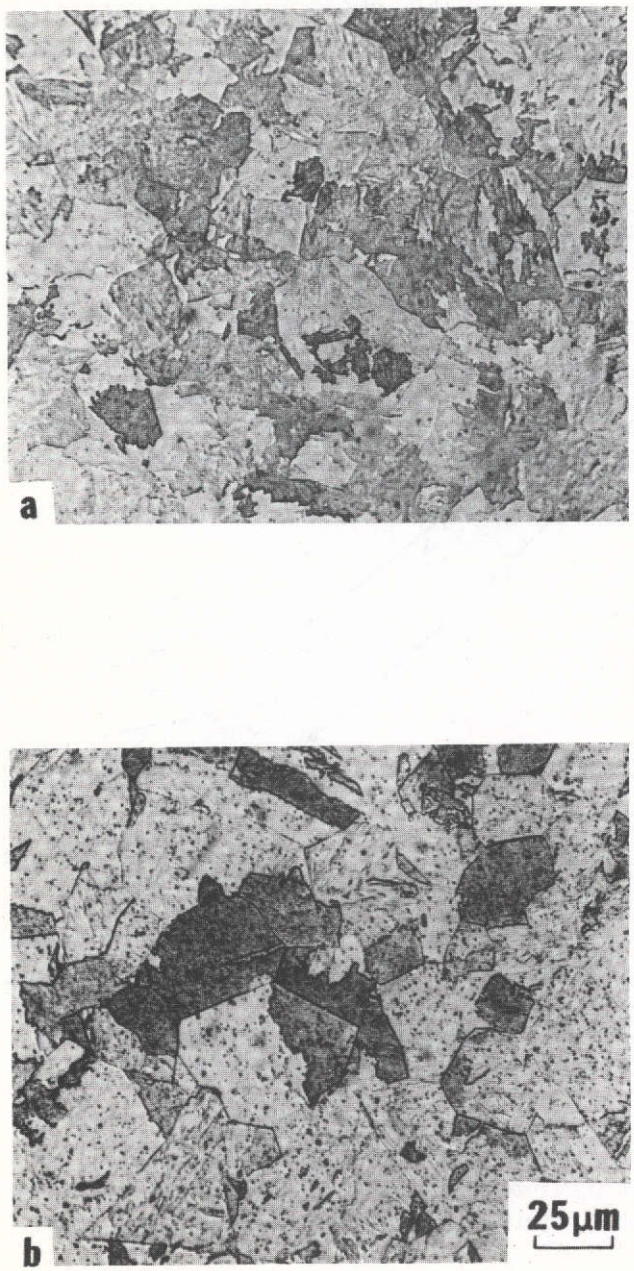

Fig. 2. Optical micrographs of as austenitized 4% Mn (a) and 8% Mn (b) alloys.

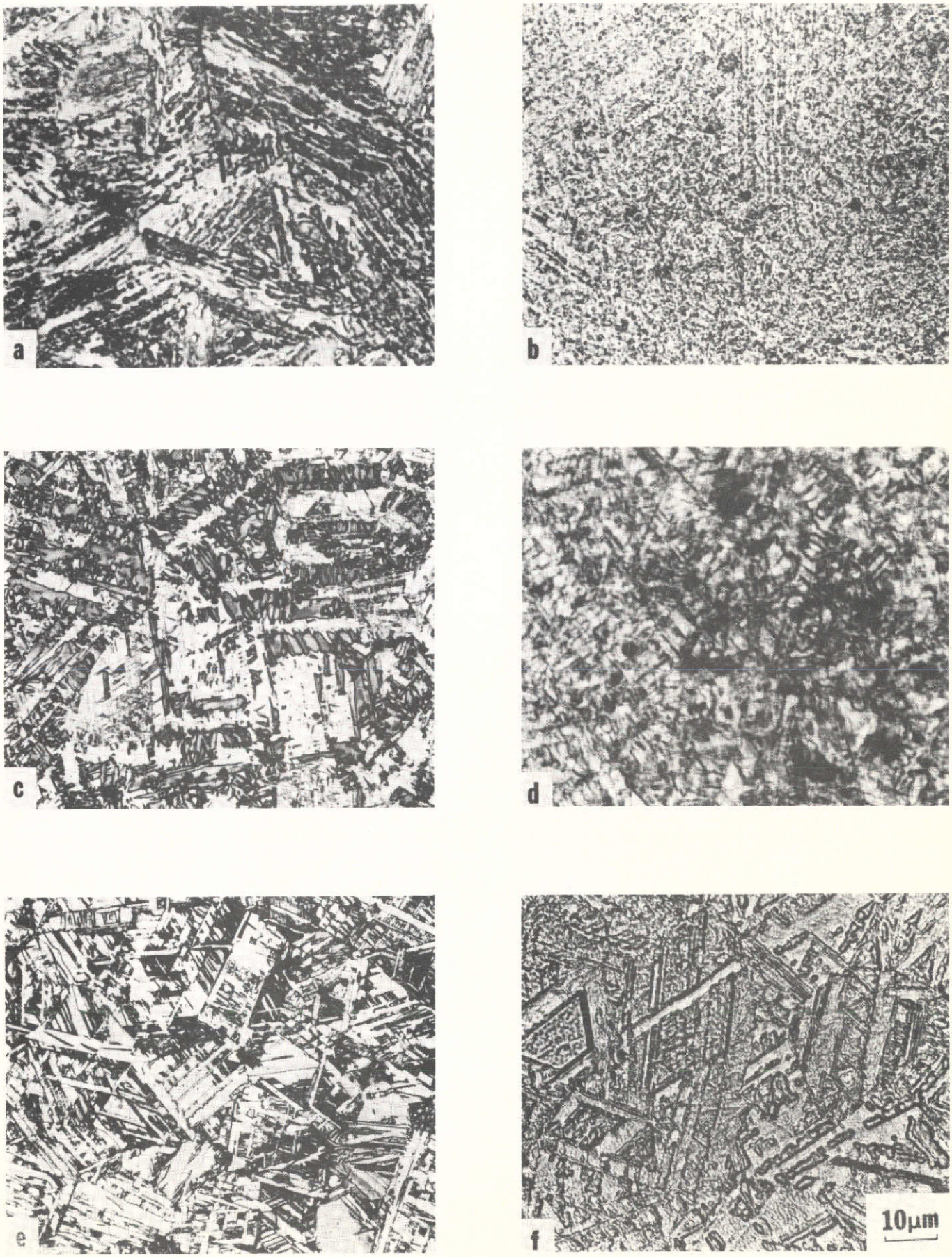

Fig. 3. Optical micrographs of a austenitized 12% Mn (a), 12% Mn-8% Cr (b), 16% Mn (c), 16% Mn-8% Cr (d), 20% Mn (e), and 20% Mn-8% Cr (f) alloys.

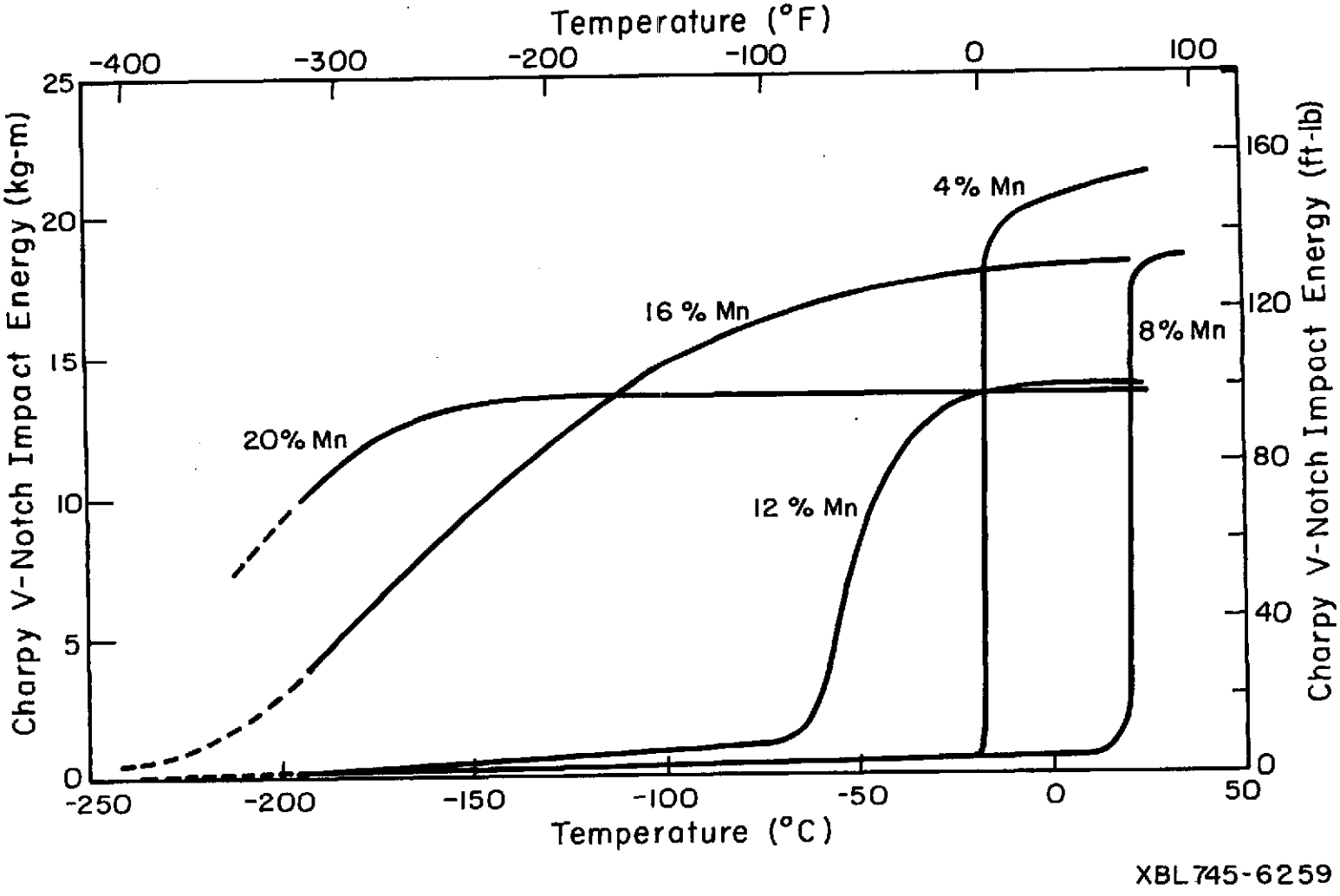

Fig. 4. Charpy V-notch impact toughness vs testing temperature for the as austenitized 4 through 20% Mn alloys without chromium.

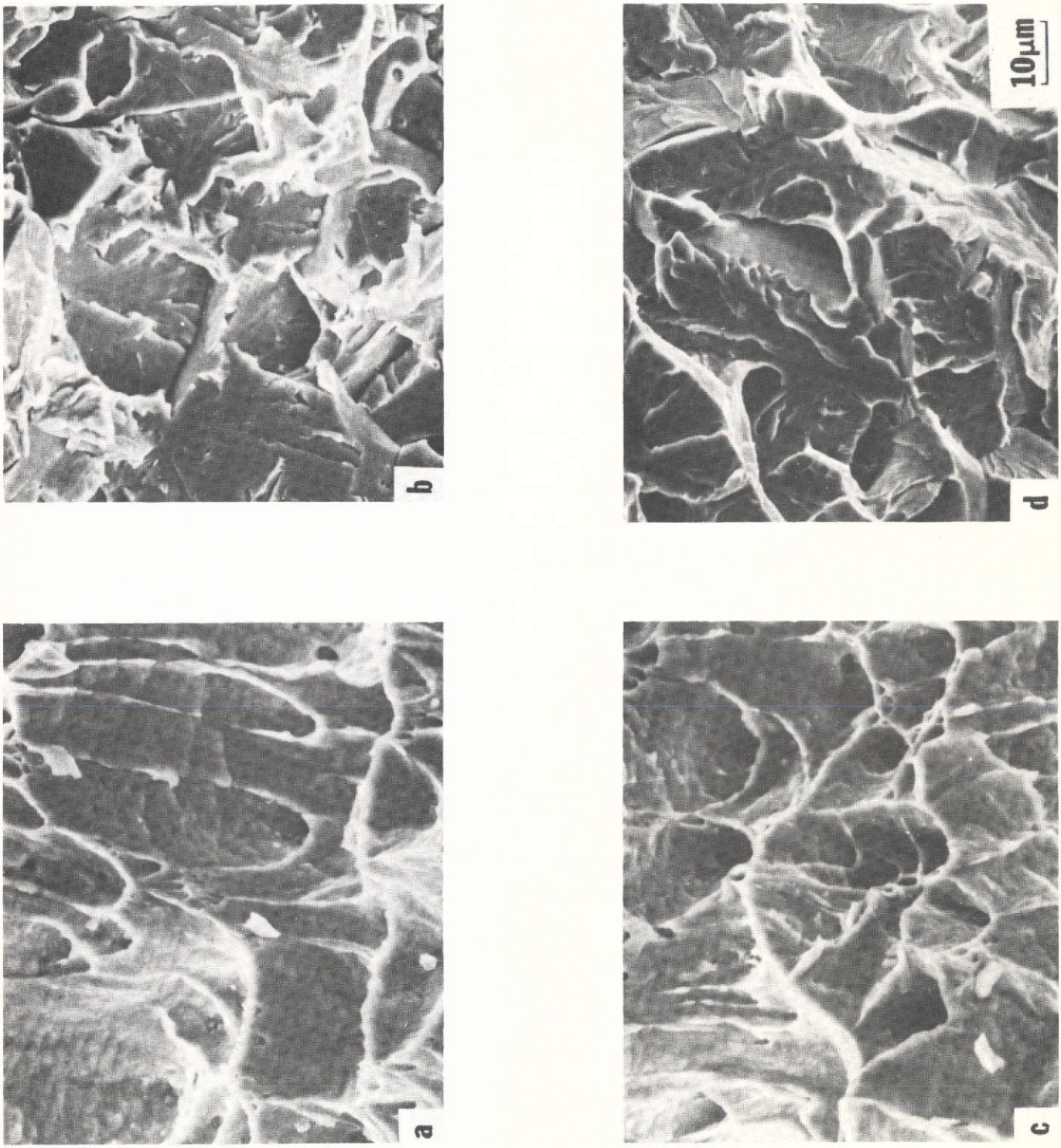

Fig. 5. Scanning electron fractographs of as austenitized 4% Mn (a) tested at 22°C, (b) tested at -196°C, and 8% Mn (c) tested at 22°C, (d) tested at -196°C Charpy fracture surfaces.

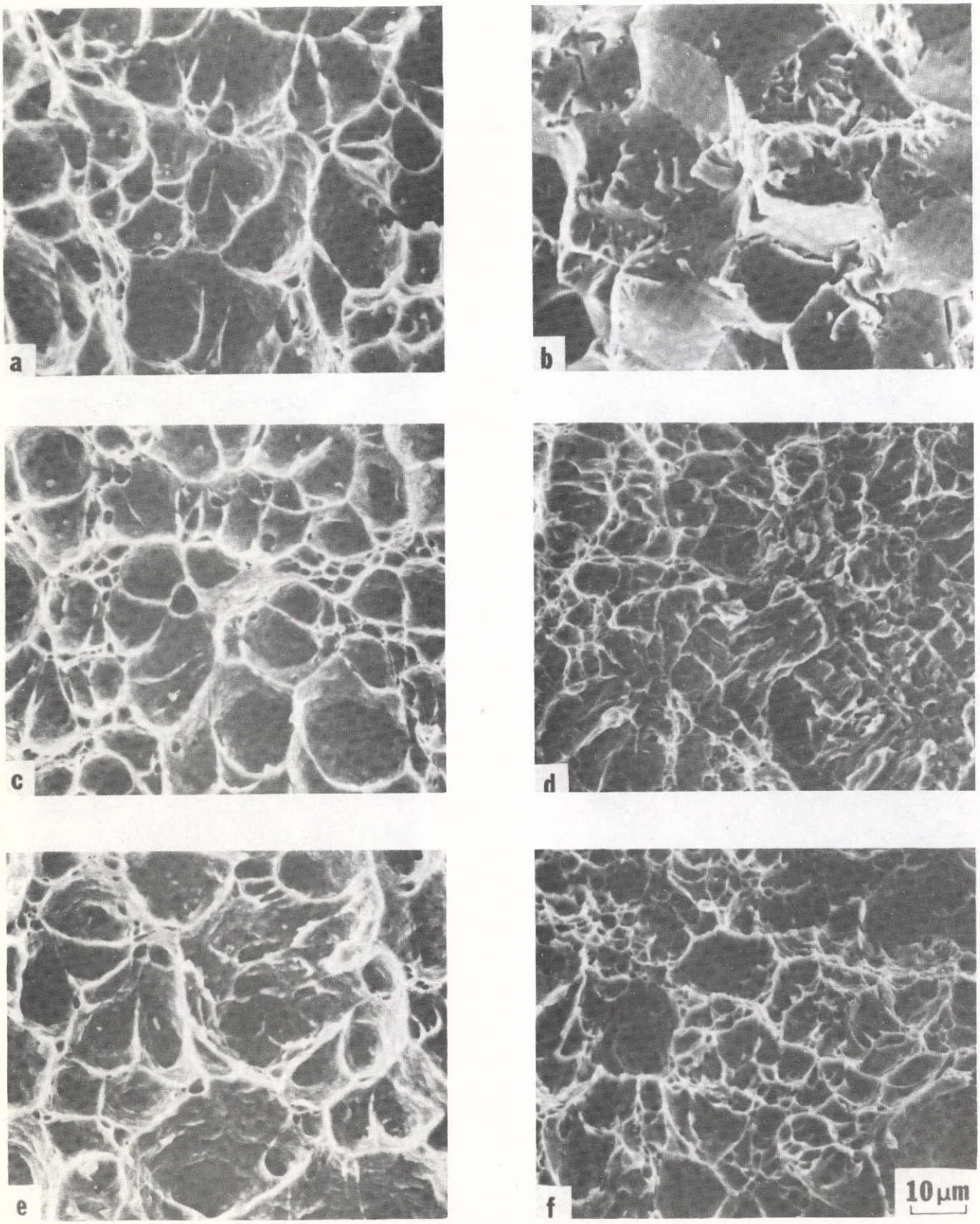

Fig. 6. Scanning electron fractographs of as austenitized 12% Mn (a) tested at 22°C, (b) tested at -196°C, 16% Mn (c) tested at 22°C, (d) tested at -196°C, and 20% Mn (e) tested at 22°C, (f) tested at -196°C Charpy fracture surfaces.

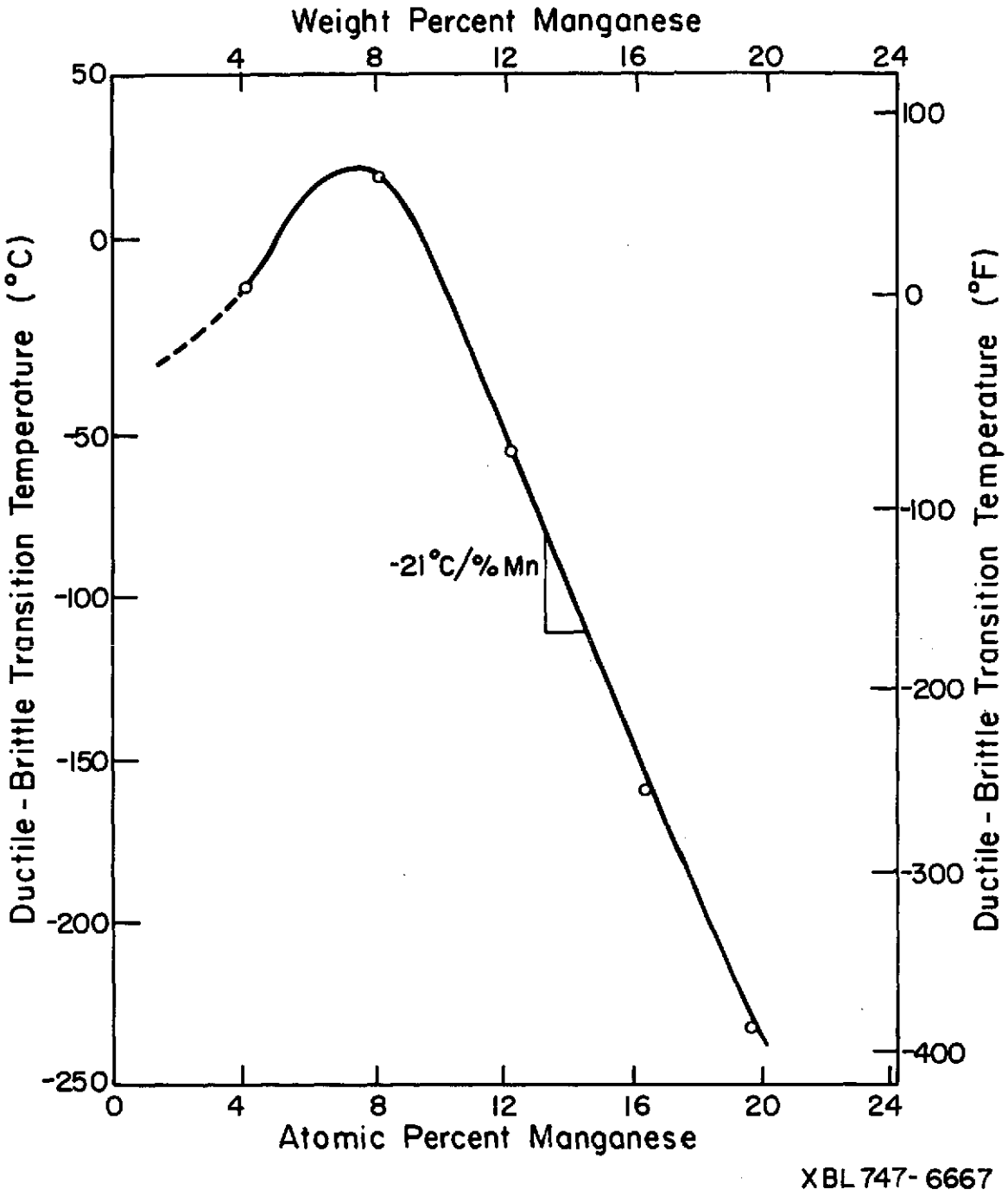

Fig. 7. Ductile to brittle transition temperature vs percent manganese in Fe-Mn alloys.

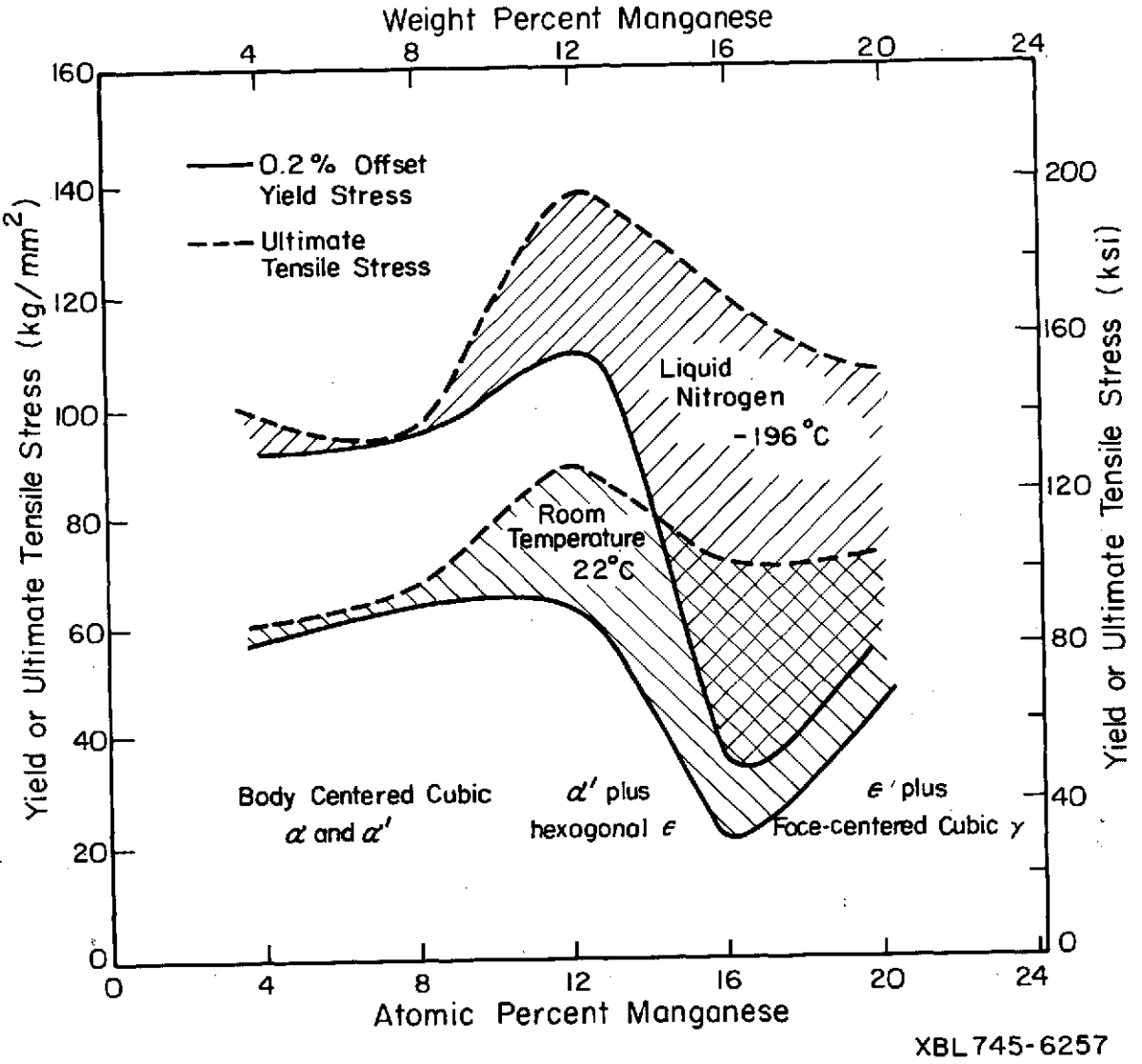

Fig. 8. Yield and ultimate tensile strength at both 22°C and -106°C vs percent manganese in Fe-Mn alloys.

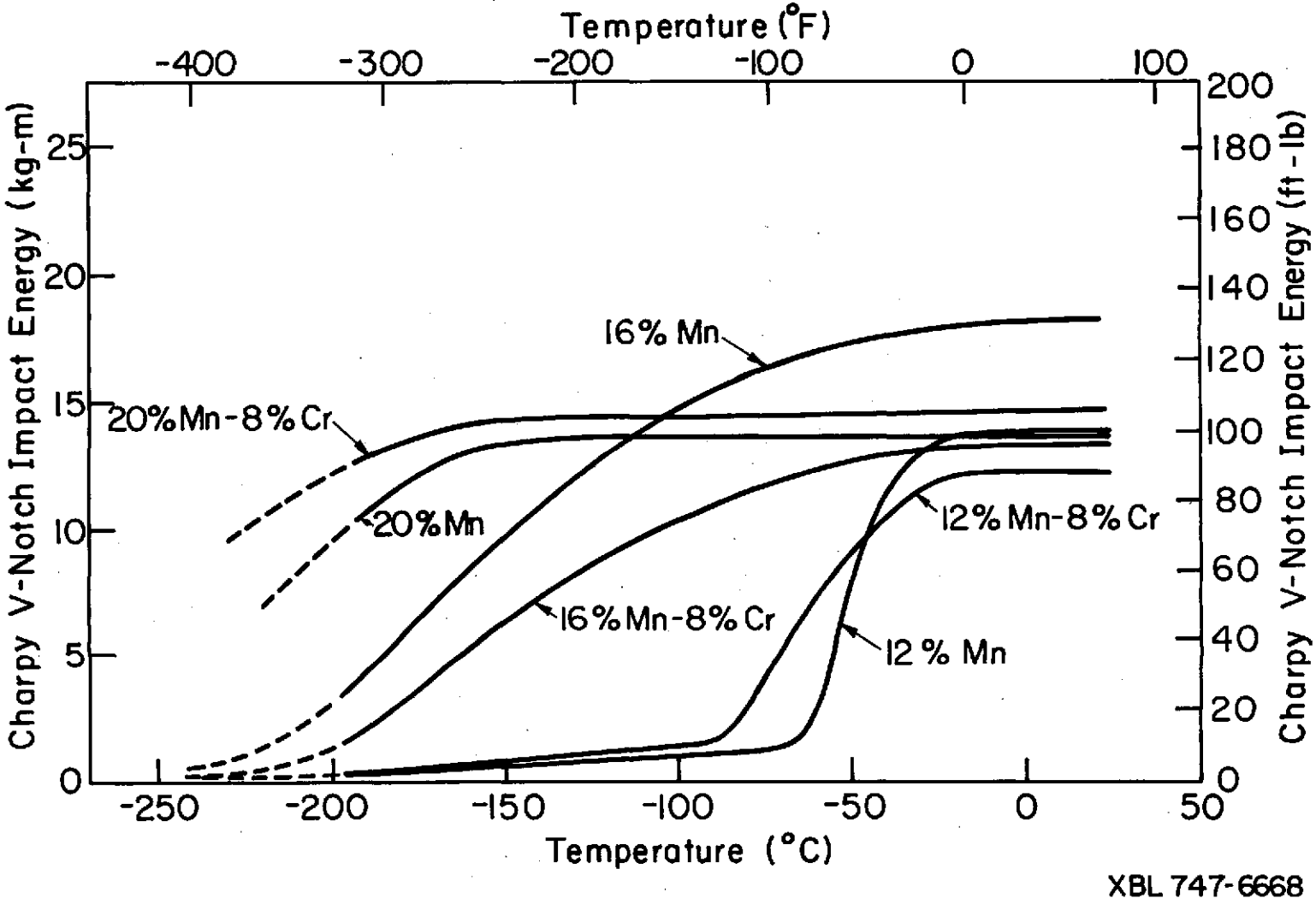

Fig. 9. Charpy V-notch impact toughness vs testing temperature for the as austenitized 12 to 20% Mn alloys with and without chromium.

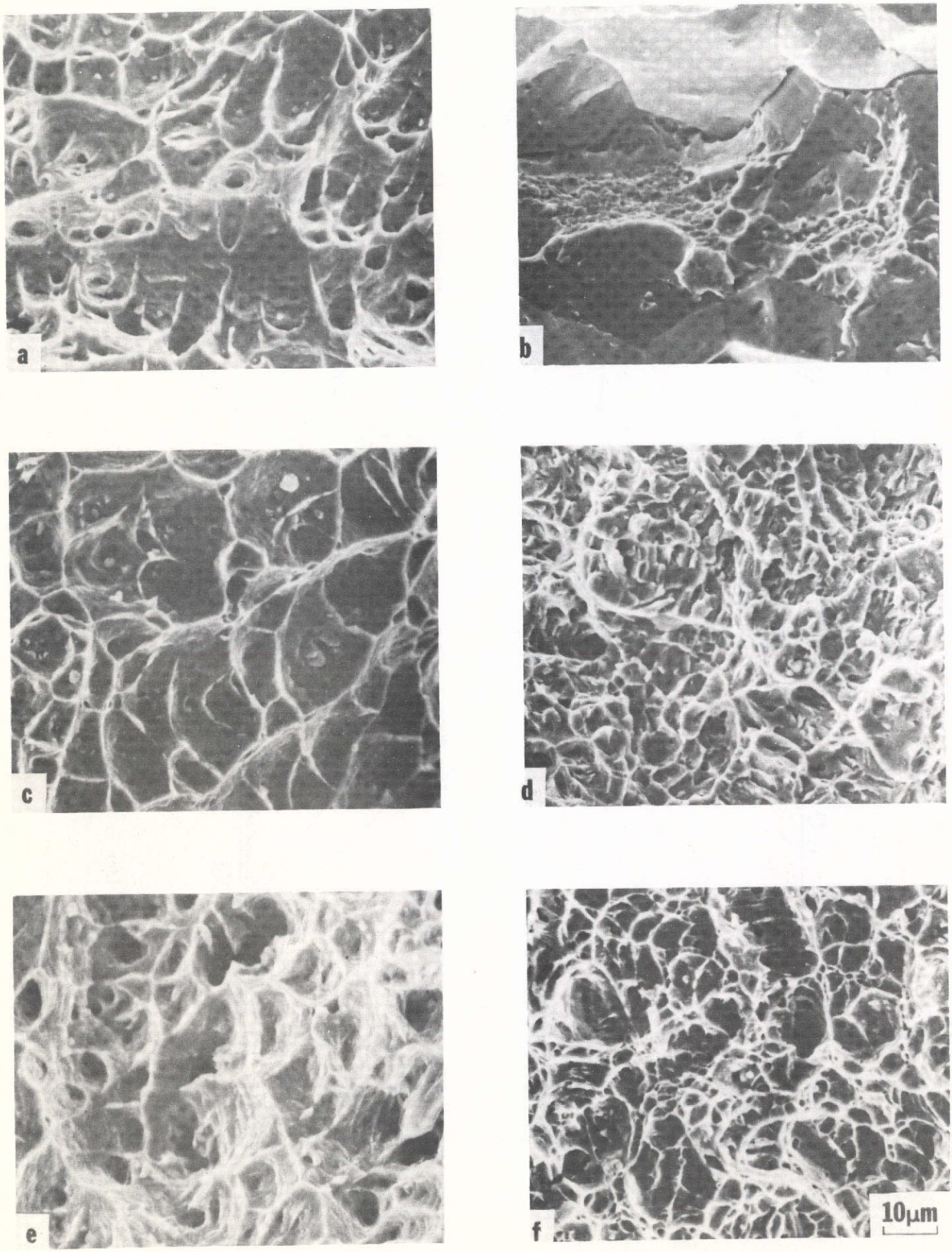

Fig. 10. Scanning electron fractographs of as austenitized 12% Mn-8% Cr (a) tested at 22°C, (b) tested at -196°C, 16% Mn-8% Cr (c) tested at 22°C, (d) tested at -196°C, and 20% Mn-8% Cr (e) tested at 22°C, (f) tested at -196°C Charpy fracture surfaces.

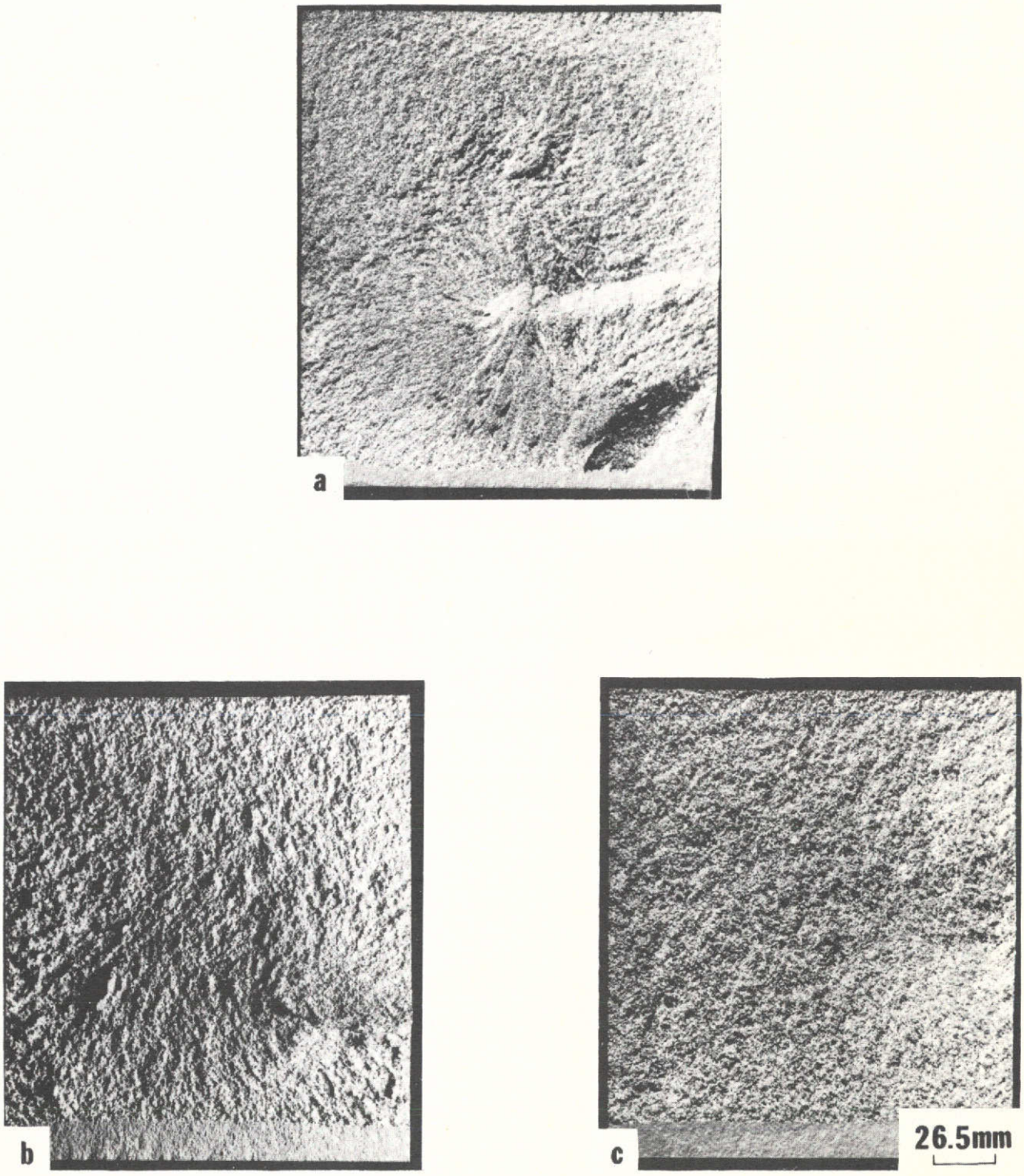

Fig. 11. Fracture surfaces of as austenitized 4% Mn (a) 12% Mn (b), and 12% Mn-8% Cr (c) fracture toughness (K_{IC}) specimens.

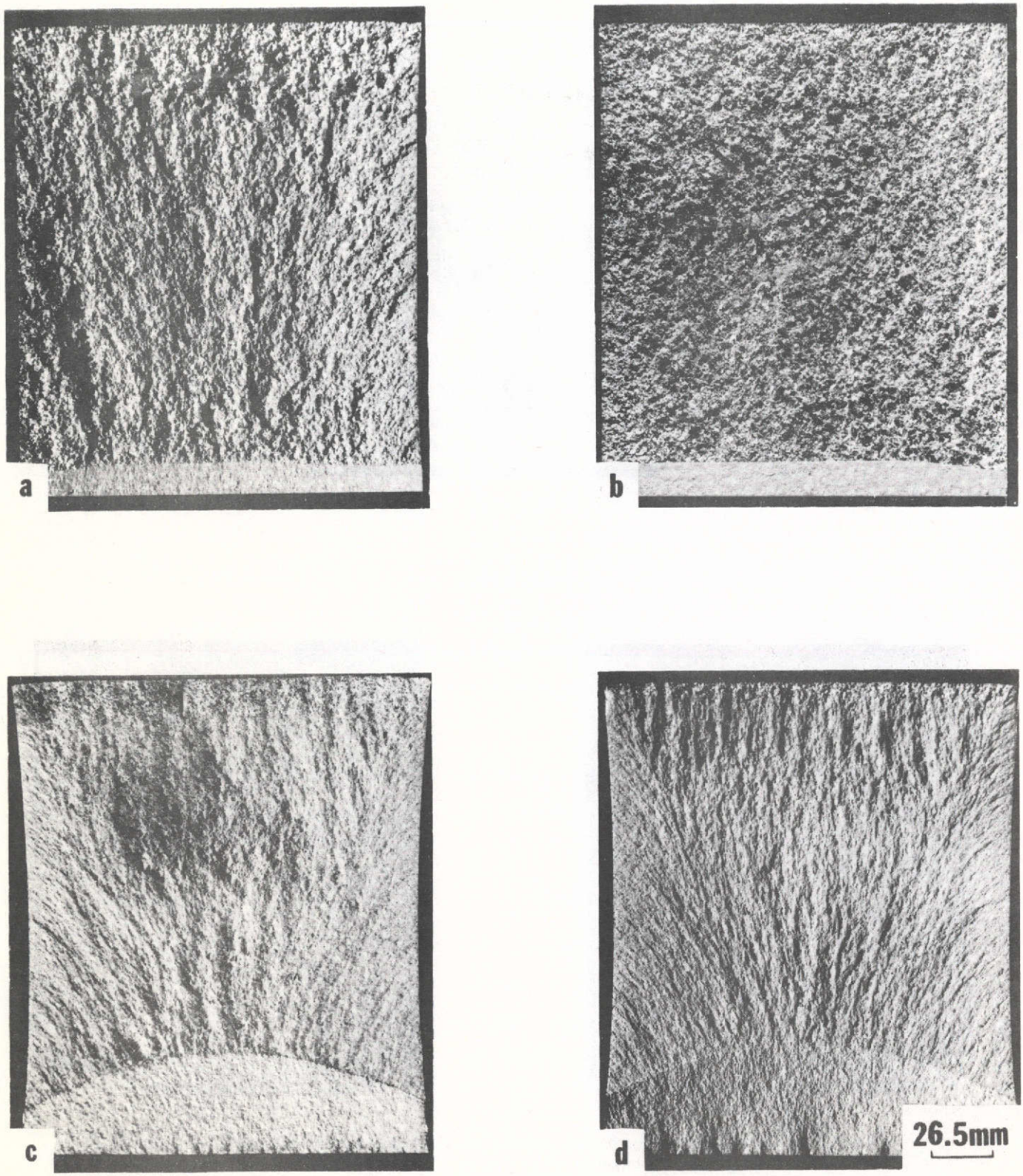

Fig. 12. Fracture surfaces of as austenitized 16% Mn (a), 16% Mn-8% Cr (b), 20% Mn (c), and 20% Mn-8% Cr (d) fracture toughness (K_{IC}) specimens.

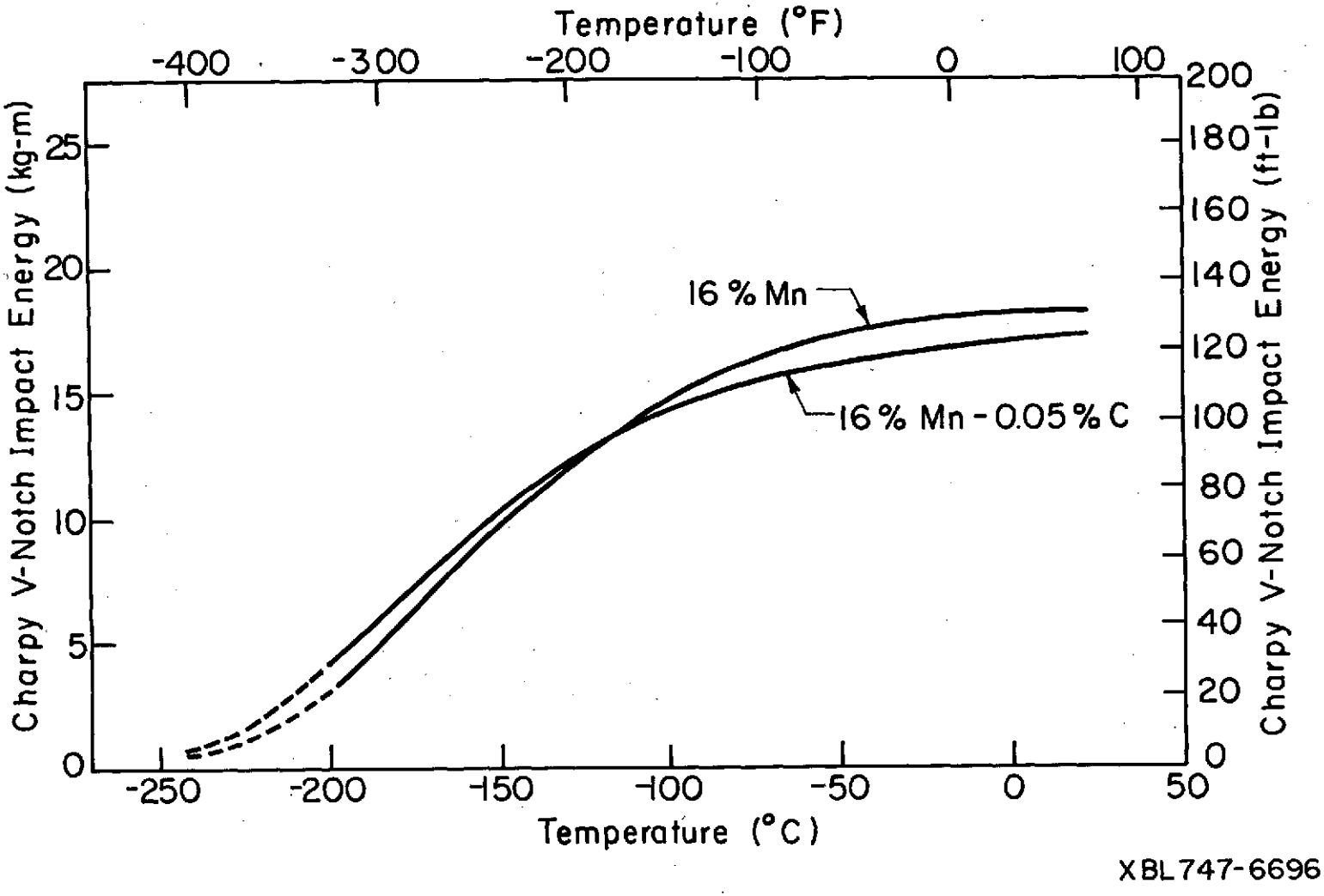

Fig. 13. Charpy V-notch impact toughness vs testing temperature for the as austenitized 16% Mn and 16% Mn-0.05% C alloys.

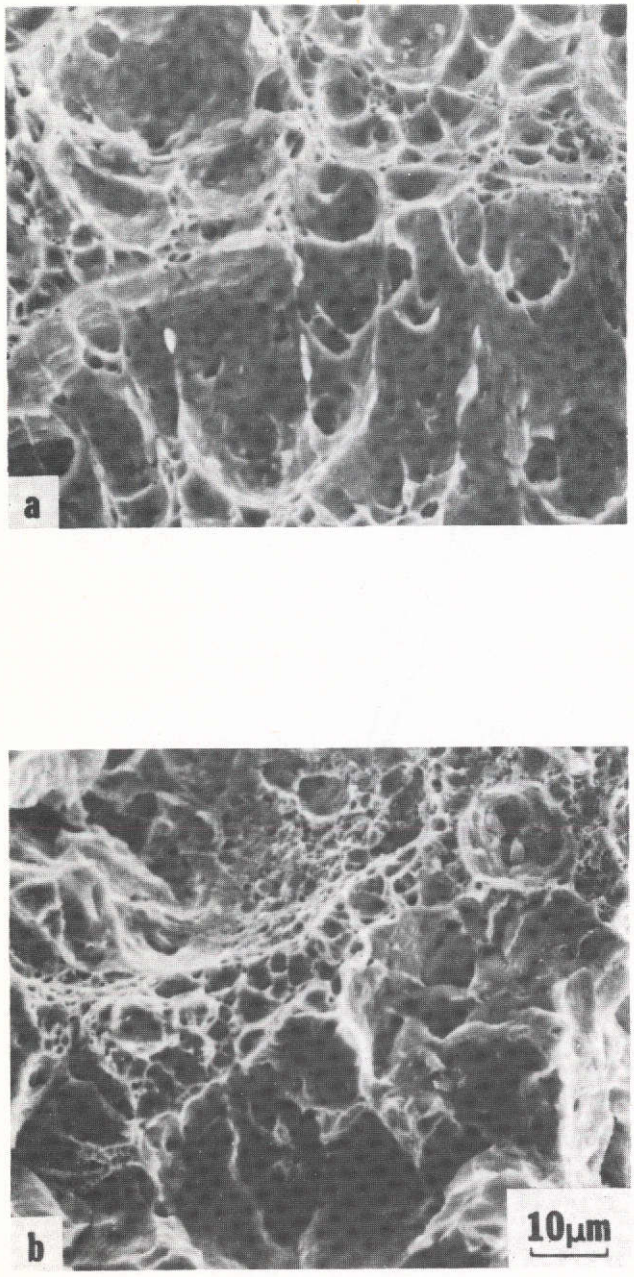

Fig. 14. Scanning electron fractographs of as austenitized 16% Mn-0.05% C (a) tested at 22°C, (b) tested at -196°C Charpy fracture surfaces.